International Journal of Material Forming (2025) 18:66
https://doi.org/10.1007/s12289-025-01933-4

ORIGINAL RESEARCH

# Analysis of tailored residual stress fields of deep rolled AA2024 sheets

Jonas Lehmann[1] · Dominik Pöltl[1] · Fabian Esterl[1] · Nikolai Kashaev[2] · Noomane Ben Khalifa[1,2]

Received: 17 June 2024 / Accepted: 15 July 2025 / Published online: 31 July 2025


**Abstract**
Deep rolling has advantages to modify local residual stresses in AA2024 sheets. A previous study about deep rolling for tailoring residual stresses [1] is extended in order to examine the homogeneity of the residual stress field. For the experimental residual stress analysis, the incremental hole drilling method with electronic speckle pattern interferometry is used with two different drill diameters. A numerical evaluation scheme is applied to simulation results of an existing process model with the aim of mimicking the experimental analysis technique. The volume under the deep rolled surface is classified in three sections based on the history of the process. Comparisons between experimental and simulative results yield a number of observations: Deeper evaluation with higher driller diameter does not come at a price of higher in-plane averaging of spatial gradients. Simulating a number of paths lower than those of the experiments shows similar homogeneity of the simulatively and experimentally analyzed stress field. Stretching the evaluation scheme from cylindrical volumes to cubic volumes shows very good qualitative agreement and validates the choice of classification.

**Keywords** Deep rolling · Residual stress modification · Residual stress analysis · Finite element analysis · Aluminum alloy

## Introduction

High strength to weight ratio materials such as AA2024 are a good choice for structural components in aerospace applications due to their high robustness towards fatigue cracking. Tailoring residual stresses in these components is a promising method to retard fatigue crack propagation [2]. These cracks are initiated near the surface. Near-surface compressive residual stresses support crack closure. In contrast, tensile residual stresses accelerate further crack opening [3]. Due to the equilibrium of stresses, residual stresses are self-balancing throughout the component. While the aim of tailoring residual stresses is compressive stresses near-surface, the location of complementary tensile stresses leads to challenges. Additionally, the time and cost required to determine the residual stresses limit the efficient application of residual stress modification techniques. Inhomogeneous residual stress fields can occur in machined materials without knowing the exact location and may require an analysis of many small volumes [4]. Therefore, the spatial resolution of the measurement volume is important when discussing residual stress states.

Deep rolling (DR) is an established technique for residual stress modification. During the DR process of a planar surface, a rolling tool presses on a small contact surface, resulting in high contact stress and yielding of the material. The plastic strains are associated with a near-surface residual stress field. The movement of the tool consists of long paths and small shifts, thereby defining a longitudinal and transversal direction. The residual stress state of deep rolled sheets is non-equibiaxial [5].

The DR process parameters which mainly influence the residual stresses are known from the literature. Altenberger [6] describes the deep rolling force as most important parameter to influence the residual stresses. Increasing the deep rolling force leads to an increase of the maximum compressive residual stress up to the material yield strength. In addition, the penetration depth increases with the DR force. The contact forces increase with the sphere diameter while the hydraulic pressure remains the same. Nagarajan

✉ Jonas Lehmann
jonas.lehmann@leuphana.de

[1] Institute for Production Technology and Systems, Leuphana Universität Lüneburg, Lüneburg, Germany

[2] Institute of Material and Process Design, Helmholtz-Zentrum Hereon, Geesthacht, Germany

et al. [7] conclude that a larger sphere diameter increases the maximum compressive residual stress and penetration depth. Beghini et al. [8] optimize deep rolling process parameters for residual stresses and show the residual stress distribution in a finite element analysis. Using a roller on the flat top surface of a cylindrical specimen, the rolling and the feed direction determine the principal residual stresses and the deep rolling force significantly affects the residual stress distribution. Alasvand et al. [9] demonstrate a higher compressive residual stress maximum as a result of a higher rolling track overlap. Denkena et al. [10] highlight the significance of the overlap factor to influence residual stresses in rotating workpieces. Multistage deep rolling in a prismatic workpiece was studied by Kämmler et al. [11]. They find that a change in plastic deformation takes place between the first repetition and third contact. Kinner-Becker et al. [12] show the influence of the track offset on the residual stresses with a simulation-based analysis of the multi-step deep rolling in a prismatic workpiece.

In the previous study [1], the DR process was investigated with focus on tailoring residual stresses in AA2024 sheet metals. The resulting shapes of the residual stress profiles and dependencies of the process parameters matched the expectations from the literature. Parameter sets could be created for tailoring residual stresses of the investigated material. The numerical simulation of the DR process also allows to show the residual stress distribution. Due to limited computing resources, only a small number of rolling pathways could be simulated and the residuals stress evaluation from the numerical model was limited.

An adequate process model of DR must include all significant phenomena influencing the residual stress field while the applied simulation technique must guarantee a minimal influence of numerical effects. Finite element method (FEM) simulations of such a process model yield a stress field for the whole modeled domain, overcoming limitations of measurement techniques. The computational resources needed for a simulation scale with the modeled number of paths. In this work, a sufficiently large number of paths is modeled that allows comparison of experimentally measured and simulatively acquired through-depth stress profiles.

This study extends the previous study about tailoring residual stresses [1] by an investigation of the homogeneity of the residual stress field. It applies an advanced post-processing evaluation scheme mimicking the experimentally measured evaluation volumes [13]. It is shown that the residual stress field for a number of paths much lower than that of the experiments exhibits homogeneity similar to the experiments.

**Table 1** Mechanical material parameters of AA2024-T3clad at 20 °C [1].

| Parameter | Young´s Modulus | Yield stress | Ultimate strength | Poisson´s Ratio | Clad layer thickness |
|---|---|---|---|---|---|
| Value | 68.9 GPa | 301 MPa | 438 MPa | 0.33 | 150 µm |

## Methods

### Experimental setup

#### Material

Aluminum sheet with a thickness of 2 mm made from AA2024 in T3 condition is investigated. The alloy has advantages in resistance to crack propagation under cyclic loading and is used in structural aircraft components [14]. The sheet metal as received has a coating with 150 µm pure aluminum as clad layer. Table 1 summarizes the mechanical properties [].

#### Deep rolling process

The experimental DR setup is as described in the previous work [1]. Figure 1 shows the hydrostatic DR tool HG6 from Ecoroll, which is installed in a CNC-controlled 5-axis milling machine. The HG6 tool has a sphere diameter of approximately 6 mm. Hydrostatic pressure is applied to the tool so that the sphere is hydrostatically mounted (see Fig. 1a). Figure 1 (b) shows that the AA2024 sheet metal specimen is clamped on a planar tool steel surface. The occurring process forces in x-, y- and z-direction are recorded by a force measurement plate from Kistler and a multi-component dynamometer up to 10 kN. The hydrostatic pressure is controlled to adjust the vertical DR force and the CNC system is used to run the process path. The specimen geometry and the process path strategy are illustrated in Fig. 1 (c). The surface treated area consists of 200 paths rolled in the rolling direction (RD, y-direction) with a distance of the tool path in x-direction of 0.1 mm. Feed velocity is kept constant at 500 mm / min. The variation in DR force is achieved by adjusting the hydrostatic pressure.

#### Residual stress analysis

X-ray diffraction (XRD) was used for near-surface residual stress determination and the incremental hole drilling (IHD) method with Electronic Speckle Pattern Interferometry (ESPI) for depth-resolved residual stress profiles.

The X-ray diffractometer Xstress G2R from Stresstech was used for non-destructive testing of residual stresses. A copper-based Cu X-ray tube with bi-axial rotation was

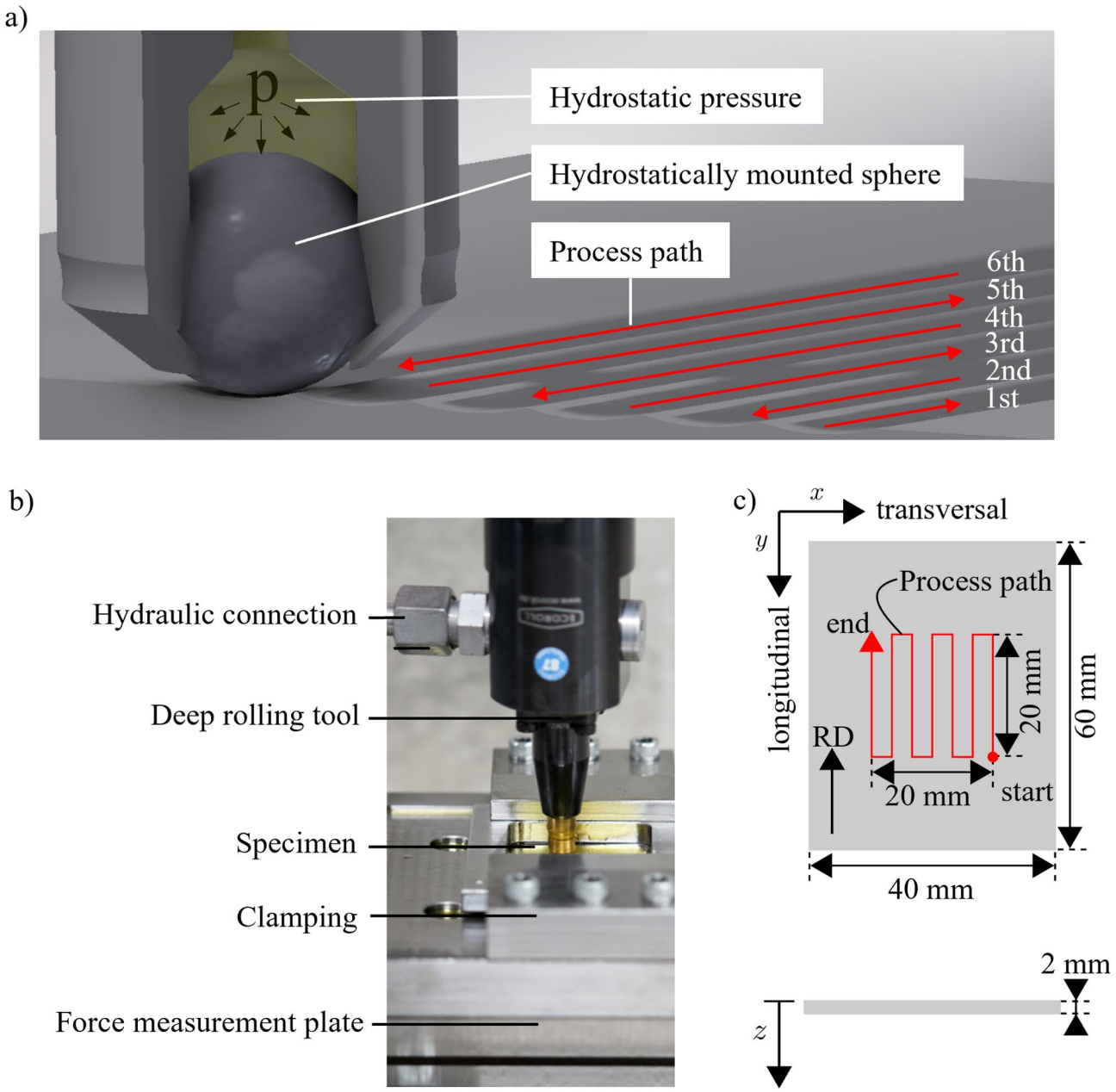


**Fig. 1** (**a**) Illustrated hydrostatic tool mounting of the DR sphere and illustrated process paths. (**b**) Experimental setup of the DR process. (**c**) Specimen geometry and process path strategy

selected. The results show the validation of the near-surface residual stresses.

The system PRISM3 from Stresstech determined the in-depth resolved residual stress profiles in a semi-destructive testing method. The system incrementally drills a defined hole into the material in accordance to ASTM E837-20 [15]. The removal of the material volume causes a surface displacement where the pixel movement within the ring around the hole is measured by ESPI [16]. The inner radius of the residual stress evaluation ring around the hole is two times and the outer radius is four times the driller radius. Using the integral method [17], residual stresses can be calculated. Iteratively, the process yields an in-depth residual stress profile. This profile is defined as "non-uniform" stresses and the IHD gives satisfactory residual stresses up to 80% of the material yield stress when the drill diameter is much smaller than the material thickness [15]. In this study, analyses are carried out with two drill diameters. The drill diameter of 0.794 mm (1/32 inch) is described in the standard [15] and the optimal depth increments are 25 µm. The second drill diameter is 2 mm, which is the same length as the thickness of the material. The depth increments near-surface are

smaller (25 µm), and increased to 100 µm for larger depths. Three residual stress at different positions analyses are performed and averaged to resolve deviations in the stress field.

## Process model

The simulation model, using an FEM framework, is set up in the commercial software Abaqus. Due to the quasi-static process characteristics, an implicit solver (Abaqus/Standard) is used to conduct the static analysis.

The modeled domain is equal to the experimental specimen described in the experimental setup. However, only a part of the experimentally processed area is simulated as to reduce computational time. Therefore, only 40 paths with a length of 5 mm were simulated, resulting in a processing area of 4 mm × 5 mm in the x and y directions, respectively. As for the boundary conditions, the bottom surface was prescribed no displacement in the z direction while the side faces were prescribed no displacement in the x and y direction. Analogous to the experimental setup, the simulation is controlled using the displacement of the sphere. To achieve similar forces as in the experiments, a correlation between displacement and reaction force is determined using a previous simulation study. To grant for the rotation of the sphere, ideal rolling without slip is geometrically derived and applied. For the representation of the contact conditions, a surface-to-surface contact is chosen, taking into account tangential behavior using penalty formulation and a friction coefficient of $\mu = 0.07$. At the end of the deep rolling simulation, all boundary conditions except for the prohibition of all translations of a single node are released as to accurately calculate the residual stress field.

Because the stress field is expected to be locally confined close to the processed surface [], a region of interest (ROI) underneath the processed surface is defined with an adequately fine mesh size. The average element size in the ROI (x × y × z) was 0.15 mm × 0.25 mm × 0.1 mm. This meshing results in 20 layers of elements along the thickness of the sheet. Outside the ROI, larger elements were tolerated. Hexagonal elements with quadratic Ansatz functions with reduced integration (C3D20R) were chosen for an optimal determination of the resulting fields.

The whole process was modeled purely mechanically with no thermal influences. The tool is modeled as a spherical, discrete rigid body. The plate's material features a linear elastic part as well as a plastic part. For the plastic part, uniaxial tensile tests have been carried out. For a summary of the material characteristics, see Table 1. Based on the measured true stress-strain values, a Ludwik curve was fitted and extrapolated. The flow curve was imported as tabular data and subsequently used for the combined isotropic-kinematic hardening, with the number of backstresses set to one.

The process model is based on previous work [1] where the experimental and simulative stress profiles showed the same tendency with a slight overestimation of the FE model in both transversal and longitudinal directions. The experimental IHD technique removes a cylindrical volume of material and determines an average stress tensor for this cylinder, thereby erasing spatial in-plane gradients. While the simulation results provide a stress tensor for each element, a numerical evaluation scheme that mimics the experimental scheme was implemented, namely virtual incremental hole drilling (VIHD) [18]. For any point on the surface, a cylinder with radius $r$ or a cube with the edge lengths $e_x$ and $e_y$ is evaluated "layer by layer" through the specimen's depth along the z-axis, resulting in through-depth profile of 20 discrete stress tensors. For each layer, all elements whose centroid lies inside the defined volume are averaged. Each mean value is associated with a standard deviation as well as minimal and maximal values. The standard deviation and the min/max values are indicators of the spatial in-plane distribution for one depth. Of course, like the experimental IHD measurements, the stress profiles at varying in-plane positions can be averaged. The resulting standard deviation is an indicator of the homogeneity of the stress field.

# Results

## Experimental results

Figure 2 shows the depth-resolved residual stress profile of the base material (BM) in x-direction (blue line) with the deviation from the minimum to the maximum value. There are tensile residual stresses of approximated 50 MPa from a depth of $z = 0.1\,\mathrm{mm}$ to $z = 0.5\,\mathrm{mm}$. The negative residual stress values $\sigma_{xx}$ show the compressive residual stresses from $z = 0.65\,\mathrm{mm}$ to the maximum of 100 MPa at the half material thickness ($z$=1 mm). IHD analyses of the reverse side show identical residual stress profiles, indicating that the residual stresses occur through the BM in an M-shape.

Firstly, the influence of the IHD drill diameter and the measurement volume on the residual stresses is experimentally investigated to validate the 2 mm IHD driller and to describe possible inhomogeneity of the residual stress fields. Furthermore, the residual stresses are considered in dependence on different processing areas. Based on both aspects, the residual stress profiles are described as a function of different DR forces.

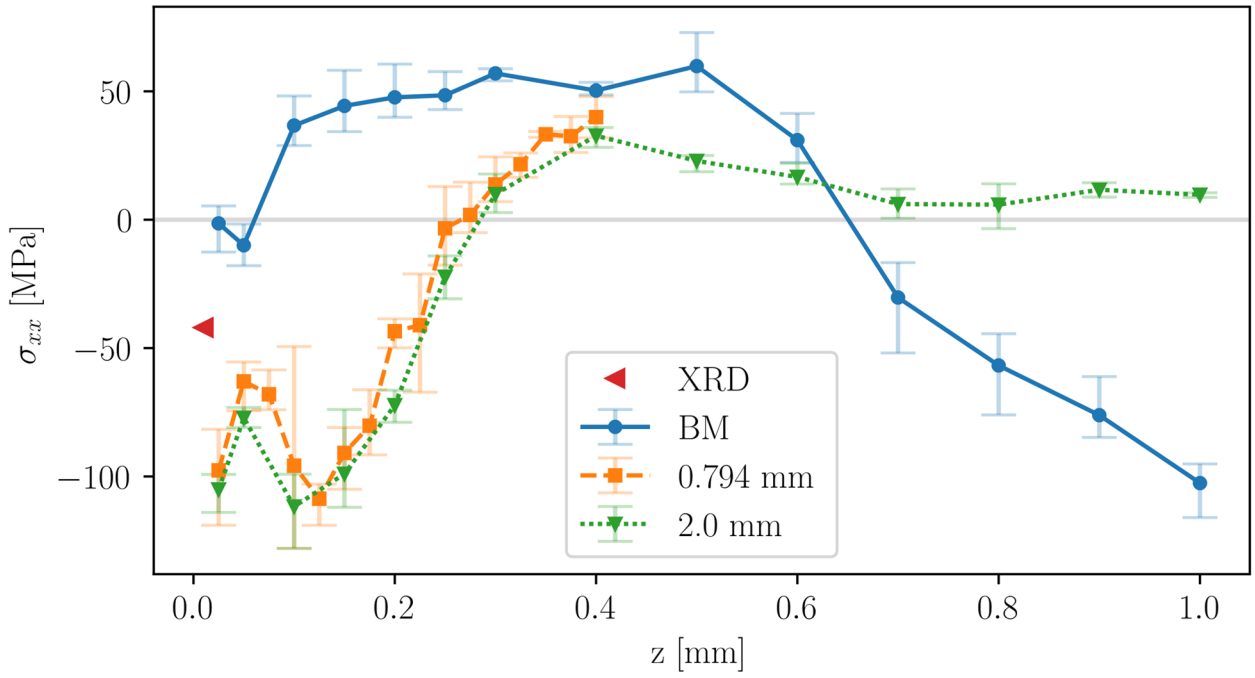


**Fig. 2** Residual stress profiles in x-direction for the as received base material (BM, blue line) and for DR with a force of 100 N, which is analyzed by XRD (red) and IHD with 2 mm driller (green) as well as IHD with 0.794 mm (1/32 inch) driller (orange)

### Residual stress analysis for different drill diameter

The experimentally determined penetration depth of the DR sphere into the material is approximately 0.01 mm for the first DR path. Following the field described in Fig. 1c and applying a DR force of 100 N, the residual stress profiles were analyzed with two different IHD drill diameters. Figure 2 compares the residual stress profiles analyzed with the 0.794 mm (1/32 inch) drill (orange line) and the 2 mm drill (green line). Both analyses show a very good agreement, so that the determination of residual stresses can also be considered reliable with the 2 mm drill, which is not recommended as satisfactory in the standard ASTM E837 [15] due to its size in relation to the material thickness. The advantage of the larger drill diameter of 2 mm is that it allows residual stresses to be determined at greater depths, so that up to half the thickness of each side of the material can be analyzed.

The residual stress profile for a DR force of 100 N reaches a maximum compressive residual stress of approximately 100 N in a depth of $z = 0.1\,\mathrm{mm}$ (see Fig. 2). The compressive residual stresses change at the penetration depth of $z = 0.3\,\mathrm{mm}$ into tensile residual stresses. The maximum tensile residual stress is approximately 40 MPa at $z = 0.4\,\mathrm{mm}$. From $z = 0.6\,\mathrm{mm}$, the residual stresses are almost 0 MPa up to the center of the material.

Near the maximum compressive stresses, the graphs of the 0.794 mm drill and the 2 mm drill deviated slightly from each other (see Fig. 2). The minimum and maximum determined residual stresses were given as deviation bars in the diagram. The scatter of the values with the smaller drill and correspondingly with the smaller residual stress analysis volume is higher. This could indicate that analysis results of smaller measurement volumes are more scattered, as less averaging is applied in the case of minor inhomogeneity of the residual stress field. The maximum deviation scatter is reached at the maximum compressive residual stress, where the inhomogeneity of the residual stress field could be slightly higher. The XRD value (red) is near the surface and makes sense as the compressive residual stress is expected to decrease here near the surface.

### Experimental classification of the deep rolling fields

The location of the IHD holes is selected in a manner that the entire evaluation ring is in the DR area. To investigate the residual stress profiles in the first paths, in the middle and in the end of the DR field, the IHD was applied in the three different DR areas. Figure 3 (a) highlights the location of the IHD holes and residual stress evaluation ring in the experiment. In the area of beginning and in the middle, there are two more holes than the expected three IHD analyses, as two measurements each led to a measuring failure.

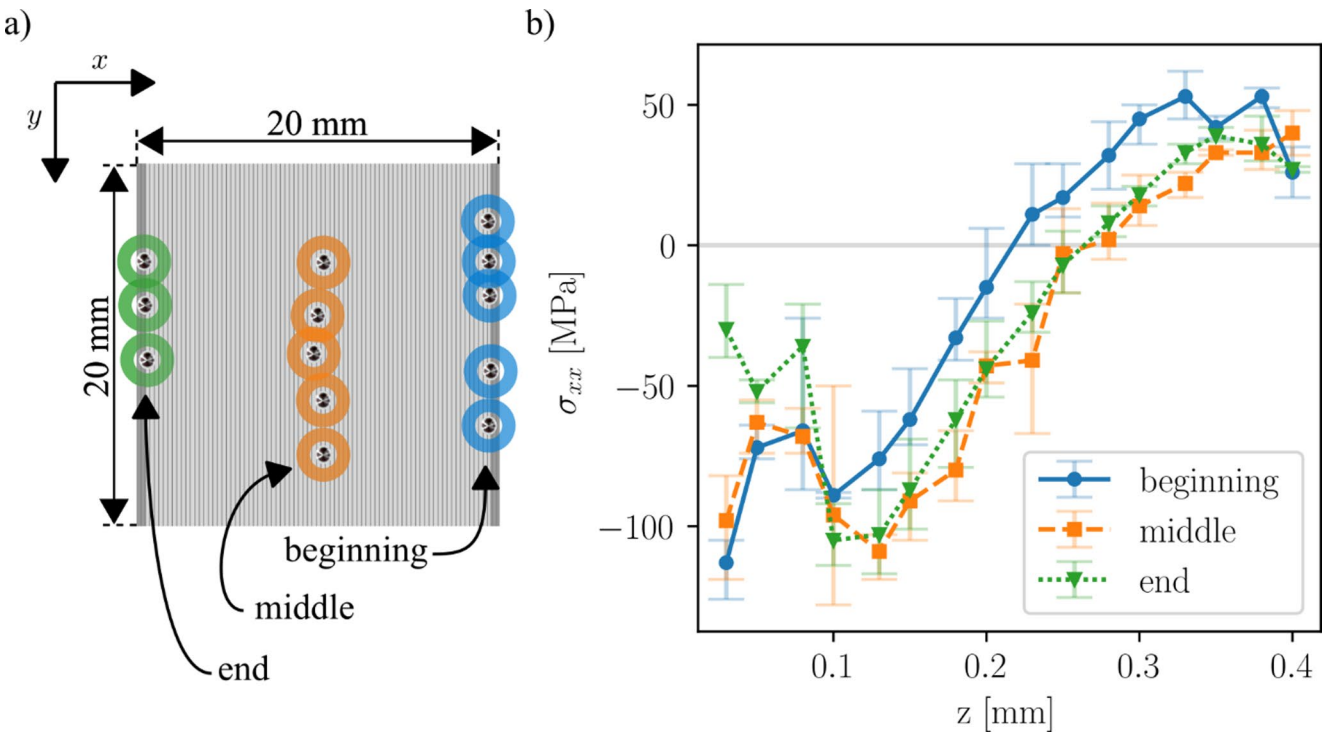


**Fig. 3** (**a**) Experimental IHD location and residual stress evaluation rings for 0.794 mm driller. (**b**) Residual stress profiles in x-direction with different IHD locations. DR force is 100 N

Figure 3 (b) shows the residual stresses $\sigma_{xx}$ over the depth $z$ for the "beginning", "middle" and "end". The shape of "beginning" is identical to that of "middle" from the surface up to $z = 0.1$ mm. After that, the residual stresses at "beginning" are approximately 10 MPa lower than at "middle" for further depths, so that the compressive residual stresses are lower, and the tensile residual stresses are higher and more similar to the values of the BM. The shape of "end" has significantly lower residual stresses than middle on the surface up to $z = 0.1$ mm. After that, the residual stresses of "end" and "middle" are identical for further depths.

### Residual stresses for different DR forces

Figure 4 explains the tailoring of residual stress profiles in x-direction as a function of the DR force and results in experimentally determined in-depth resolved residual stresses for the DR process in combination with the AA2024 sheet metal. All residual stress profiles have the same characteristics with maximum compressive stresses and penetration depth. Higher DR forces lead to higher maximum compressive residual stresses. The limit seems to be at $\sigma_{xx} = -150$ MPa and is at the depth $z = 0.15$ mm. The penetration depth increases from $z = 0.15$ mm at 50 N via $z = 0.30$ mm at 100 N, $z = 0.38$ mm at 150 N and $z = 0.45$ mm at 200 N up to $z = 0.55$ mm at 300 N. The deviation bars in the diagram show the minimum and maximum measured residual stresses.

Table 2 summarized the hydrostatic pressure and the correlated DR force together with the close to the surface XRD residual stresses $\sigma_{xx}$. Higher hydrostatic pressure and consequently DR forces lead to less compressive residual stresses. This supports the statement from Fig. 4. Higher forces shift the curve to the right, so that the residual stresses increase near the surface.

The experimental results in Fig. 4 show the same tendency as the simulation results from previous work [1]. The simulated transversal maximum compressive residual stress in Fig. 6 of the previous work [1] also reached a limit for higher DR forces. However, it should be noted that the there is an absolute difference in maximum compressive residual stress of about 85 MPa. This relative error of about 40% is due to limitations in the FE model, mentioned in the discussion section. The simulated penetration depth in Fig. 7 of the previous work [1] also increases linearly similar to the experimental results. Again, the simulated penetration depths are 25% higher than the experimental results shown in Fig. 4.

## Simulative results

In this work, three numerical evaluations are done: (a) for a fixed radius in six cylinders with random coordinates of the

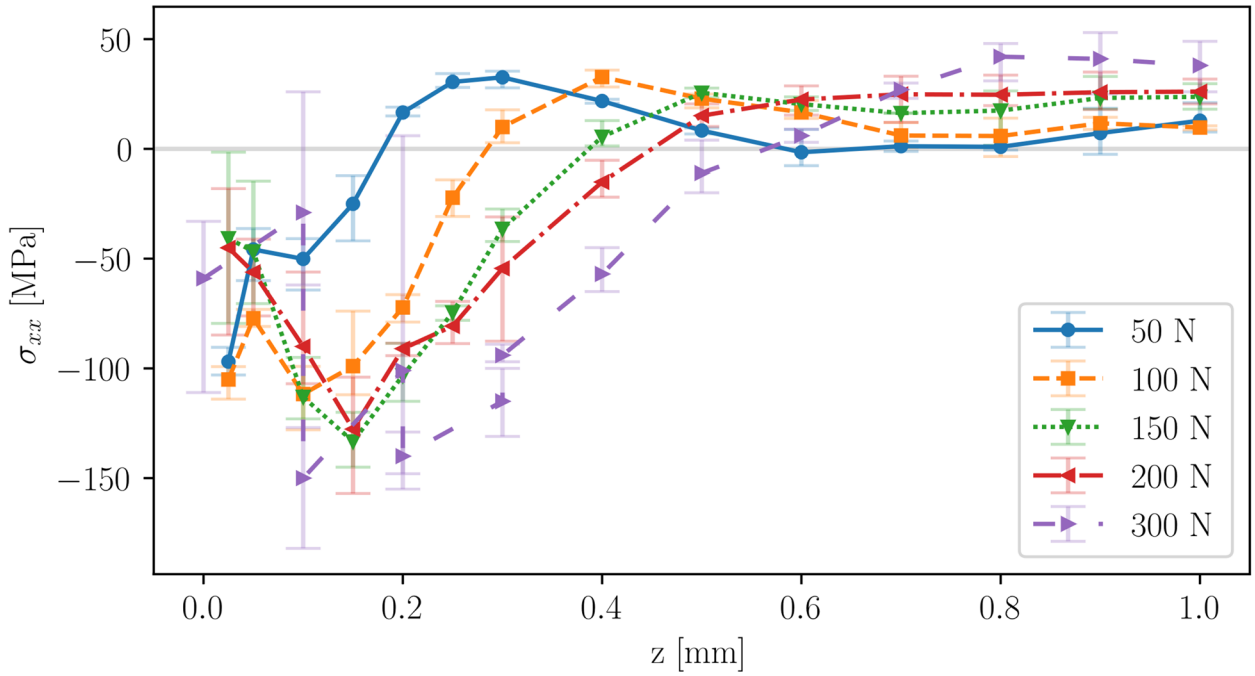


**Fig. 4** Residual stress profiles in x-direction for different DR forces. Residual stresses were determined by IHD with 2 mm driller

**Table 2** Near-surface residual stresses in x-direction analyzed with X-ray diffraction for different hydrostatic pressure parameters and consequently DR forces

| Hydrostatic pressure | *n*.a. | 39 bar | 59 bar | 79 bar | 119 bar |
|---|---|---|---|---|---|
| Deep rolling force | 50 N | 100 N | 150 N | 200 N | 300 N |
| $\sigma_{xx}$ from XRD | -61 MPa | -43 MPa | -37 MPa | -27 MPa | -17 MPa |

center; (b) for a set of increasing radii in the middle of the processed surface and (c) for three cubic volumes including the first five paths, the middle and the last five paths. Figure 5 (a) and (b) shows the three evaluations in the processed surface.

Each cylindrical evaluation volume is defined by the x and y coordinates on the specimen's surface. Setting the diameter of the cylinder to $d = 0.8$ mm, equaling the diameter of the experimental IHD measurements, six cylinders can be positioned in the volume under the treated surface such that the minimal distance between each cylinder's centers is twice the diameter.

A mean stress profile is calculated as the mean of the six individual stress profiles. Figure 5 (c) depicts the normal component in x-direction. It exhibits a maximal compressive stress of $\sigma_{min,xx} = -273.8$ MPa right in the first layer of elements for a depth of $z = 50$ µm. With a linear interpolation between the 20 values along the depth, the first sign change happens at $l_{pen} \sim 0.4$ mm. Far beyond the depth that an IHD measurement can reach, the simulatively acquired mean stress profile exhibits a second sign change at $l_2 \sim 1.5$ mm. The standard deviation - in this case representing differences between the profiles of different cylinders - has a maximum of $|\sigma_{std,xx}| = 25$ MPa. This low deviation indicates the homogeneity of the stress field in the volume underneath the treated surface.

The assumptions behind the stress determination by IHD give rise to a relation between the drill diameter $d$ and the maximal depth of the blind hole $z_{max} = 0.5\,d$. While a larger drill diameter will allow for deeper evaluation, it will also average out more of the in-plane spatial gradients. The proposed numerical evaluation scheme determines the full through-thickness stress profile for any radius. To investigate the influence of the diameter of the radius, four cylinders, each with an in-plane center in the middle of the treated surface and with radii between $r_{min} = 0.4$ mm and $r_{max} = 1.0$ mm, were evaluated. With stress values similar to those shown in Fig. 6 (a), differences between the four stress profiles can be visualized in an improved fashion by the difference $\Delta\,\sigma_{xx}(z; r_i) = \sigma_{xx}(z; r_i) - \sigma_{xx}(z; r_{max})$.

This sets the stress profile for $r = 1.0$ mm as the reference profile and is shown in Fig. 6 (b). The difference between the profiles is mostly negative for $z^* \leq 0.75$ mm while the associated standard deviations render the possibility of sign changes throughout the thickness. The interpretation again

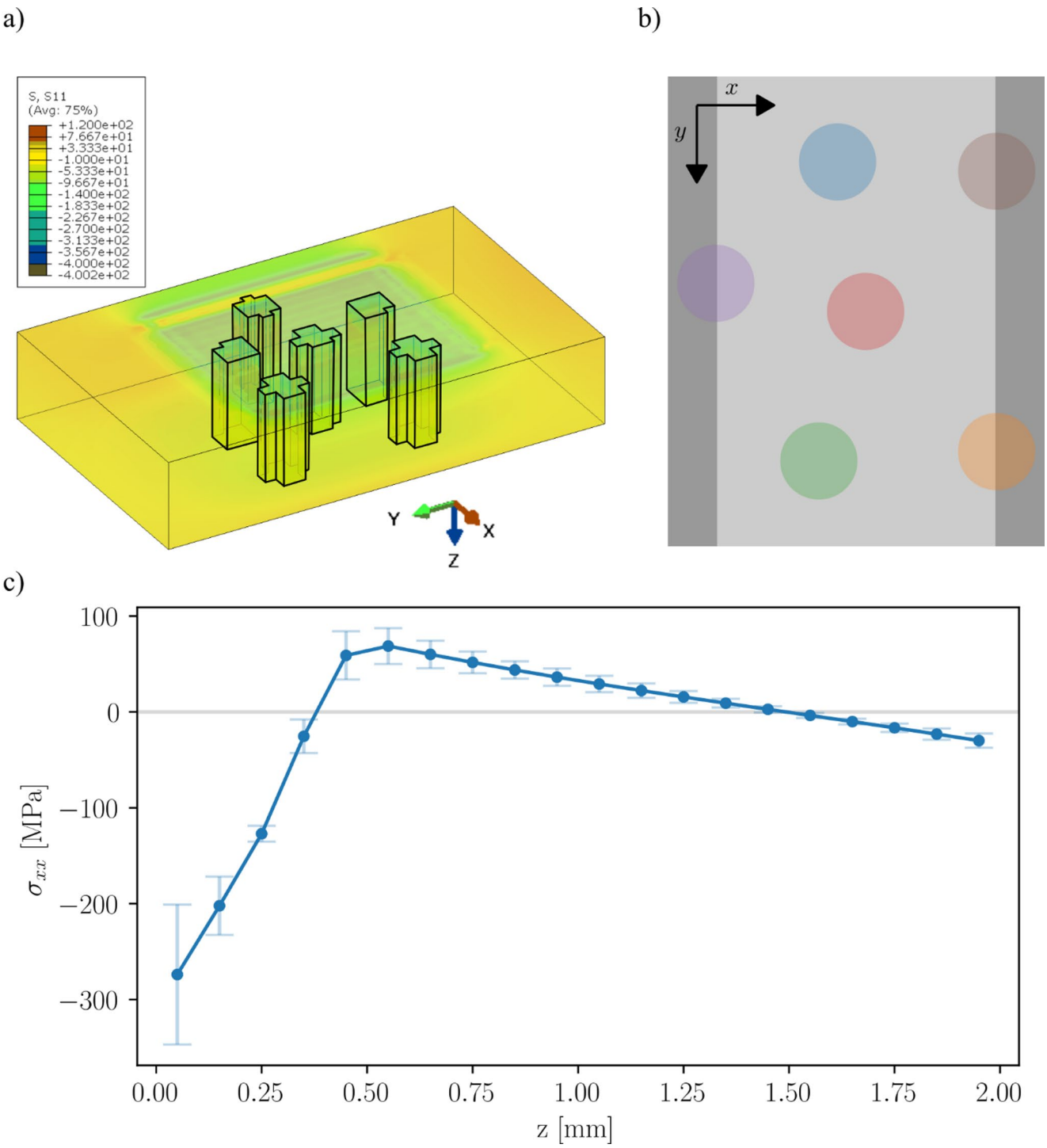


**Fig. 5** (**a**) Region of interest with six randomly placed cylindrical evaluation volumes. (**b**) In-plane positions of the evaluation volumes. (**c**) Residual stress profile in x-direction, averaged over the six cylindrical evaluation volumes

leads to the spatial in-plane gradients, but also pins down their influence on the mean stress in the evaluation volume.

Lastly, three cubic volumes are evaluated: The first features the volume underneath the first 5 paths (beginning), the second features the volume underneath paths 6 to 35 (middle), and the end, similar to the start, features the volume underneath the last five paths. For all three, the averaging in each layer features many more elements. The calculated mean and standard deviation yield good indications of the homogeneity of the stress field underneath the treated surface. All three profiles are shown in Fig. 7.

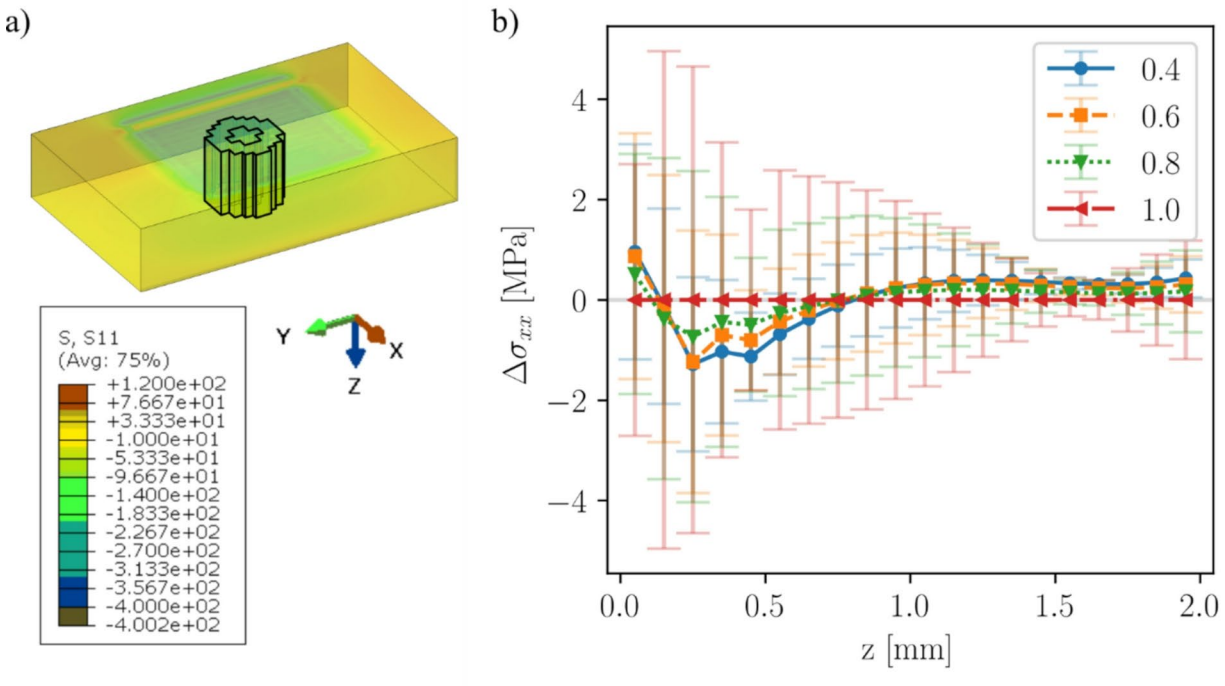


**Fig. 6** (**a**) Region of interest with cylindrical evaluation volume for smallest and largest radius. (**b**) Residual stress profiles and standard deviations in x-direction for different radii

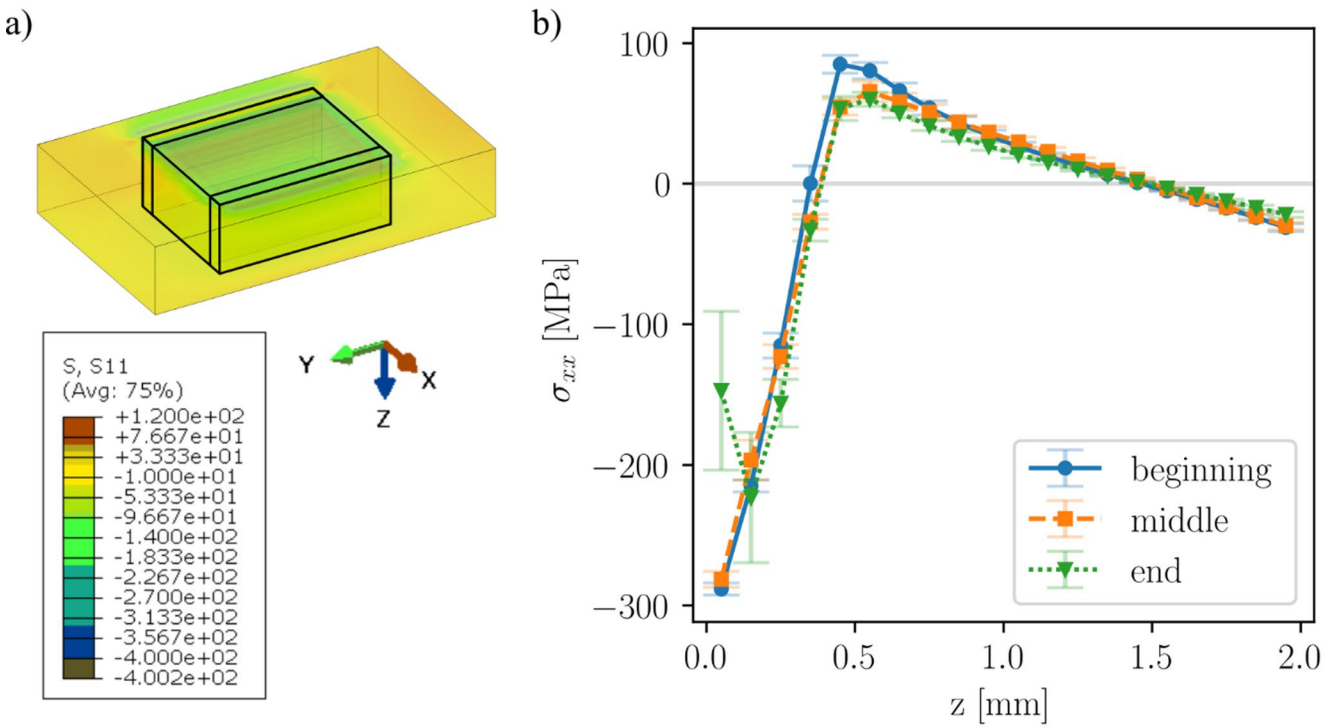


**Fig. 7** (**a**) Region of interest with three cubes indicating beginning, middle and end volumes. (**b**) Residual stress profiles in x-direction for three cubic evaluation volumes. The deviation indicated is from minimum to the maximum value

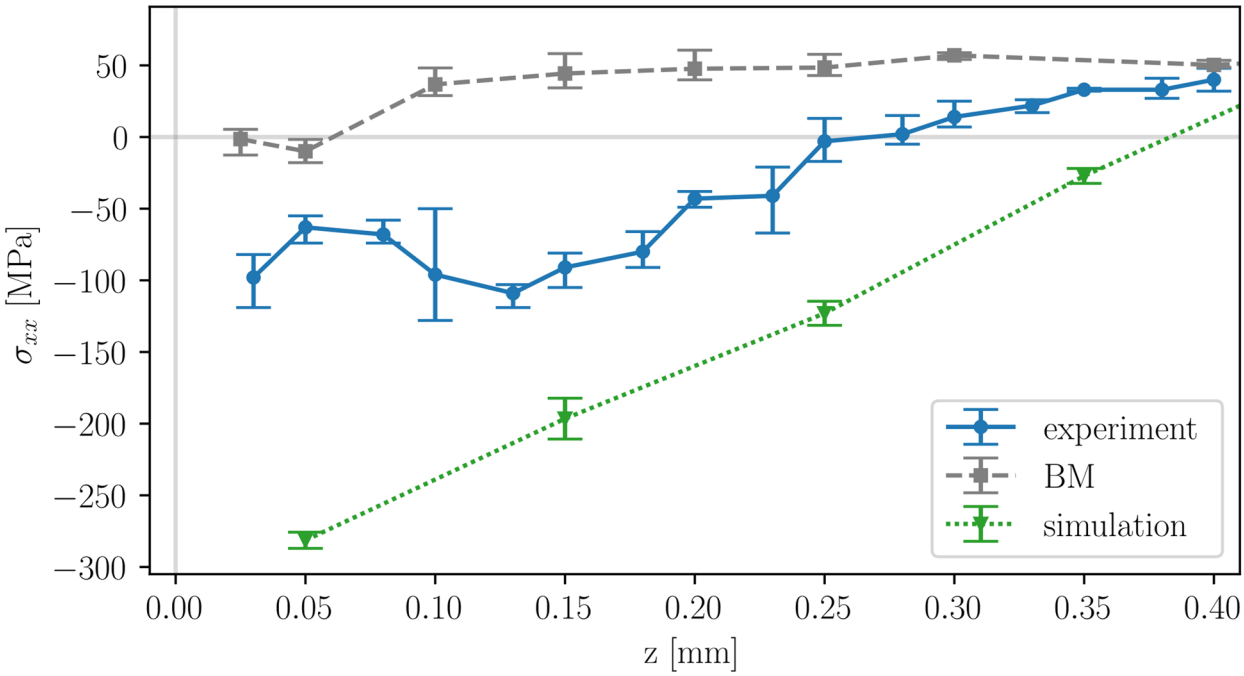


**Fig. 8** Comparison of experimental and simulative residual stress profiles in x-direction after DR with a force of 100 N

The profiles for beginning and middle exhibit maximum compressive stresses of $\sigma_{min,xx} = -280$ MPa for a depth of $z$ =50 µm. The first value closest to the surface for the end profile shows a deviation towards tensile of 130 MPa. The change from compressive to tensile stresses is determined to be at $l_{pen} \approx 0.4$ mm for all profiles. It is notable that the volume featuring the first rows exhibits a maximum tensile stress which is $\approx$ 20 MPa higher than the middle field. All three profiles show a second sign change at $l_2 \approx$ 1.5 mm. While the beginning and middle feature very small standard deviations, indicating high in-plane homogeneity, the field underneath the final paths exhibits maximal standard deviations close to the surface of $\sigma_{std,xx} \approx$ 100 MPa. This indicates temporally increasing homogeneity: While the stress field in the volume under the first paths was mainly influenced by these paths, neighboring paths that came afterward also had an influence. The stress field in the volume under the last paths was already influenced by previous paths but will not be influenced by future paths. The middle lends itself as a good representation of the average stress field induced by deep rolling.

## Discussion

In previous work, efforts to validate the process model have been taken [1]: For a given deep rolling force, experimental stress profiles were obtained by IHD and simulative profiles were obtained by the evaluation along a path, touching one element per layer along the depth. The simulative profile was (mathematically) underestimating the stresses. Using the proposed numerical evaluation scheme, the aim was to reduce the delta between experimental and simulative results. Yet, the difference in maximal compressive stress is $\sigma^{sim}_{min,xx} - \sigma^{exp}_{min,xx} =$ -220 MPa (see Fig. 8).

A critical investigation of this difference leads to three possible sources of error in the process model: The physical specimen features a clad layer of pure aluminum with a thickness (as received) of 150 µm. This layer of a material softer than the investigated alloy is not included in the model. Mechanical reasoning suggests, that an included clad layer would act as a damping on the residual stress generation and thus (mathematically) increase the minimal value of the stress profile. A second source of error is the simplified modeling of surface friction: While the real process features non-perfect surfaces with asperities and friction with stick-slip phenomena, the model uses Coulomb friction with an isotropic coefficient µ and no slip. Including a more advanced friction mechanism is expected to also act as

a dampening, further (mathematically) increasing the stress profile. The third source of error is the numerical state of the simulation: Increasing the mesh density in the treated volume beyond the threshold of mesh independence would discretize spatial gradients better than the current mesh does. While this will not change the average of the in-plane stress field, it is expected to give a better indication of the standard deviation. Finally, it must be noted that no hierarchy among the error sources is proposed.

Despite the overestimation of compressive residual stresses using VIHD when compared to the experimental values, the proposed VIHD scheme improves the comparability of the simulative results to the IHD procedure. Stretching the VIHD scheme from cylindrical evaluation volumes to the evaluation of the cubic beginning/ middle/ end volume shows excellent qualitative agreement, especially regarding reduced compressive residual stresses near-surface for the end.

The proposed classification of the volume under the treated surface into beginning, middle, and end is valid due to the characteristics in the residual stress field. Therefore, this classification can be used to access the necessary number of paths needed to correctly represent the process characteristics. Based on this analysis, the assumption of periodicity of the residual stress field in the middle of the processed area is valid.

Furthermore, both the experiment and simulation indicate a significant homogeneity of the transversal stress component in the middle of the processed area. An investigation of the influence of the driller diameter shows that this deeper evaluation does not come at a price of higher in-plane averaging of spatial gradients. The process is capable of tailoring homogeneous compressive residual stresses transversal to a rolling direction for the investigated set of parameters.

## Conclusions

The previous study about deep rolling for tailoring residual stresses [1] is extended to investigate the homogeneity of the residual stress fields. For this purpose, an advanced post-processing evaluation scheme mimicking the experimentally measured evaluation volumes is applied. The results of the experimental and numerical investigation lead to following conclusions:

- The experimental data is extended by residual stress profiles and X-ray diffraction values for deep rolling using different deep rolling forces.
- The volume under the treated surface was classified as beginning / middle / end on the chronological order of the process.
- Deeper evaluation, enabled by larger driller diameter, does not come at a price of higher in-plane averaging of spatial gradients.
- Stretching the VIHD scheme from cylindrical evaluation volumes to the evaluation of the cubic beginning / middle / end volume shows very good qualitative agreement, thus validating the choice of classification.
- The simulated residual stress field for a number of paths much lower than that of the experiments exhibits homogeneity similar to the experiments.

Future work will focus on exploiting the homogeneity of the residual stress fields to make numerical simulation of large deep rolled fields more efficient.

**Acknowledgements** The authors kindly acknowledge the support from technical staff at Leuphana University Lüneburg and HEREON.

**Author contributions** All authors contributed equally to this work.

**Funding** Open Access funding enabled and organized by Projekt DEAL.

**Data availability** Data sets generated during the current study are available from the corresponding author on reasonable request.

## Declarations

**Declaration of competing interest** The authors declare that they have no known competing financial interests or personal relationships that could have appeared to influence the work reported in this paper.



## References

1. Lehmann J, Keller S, Esterl F et al (2024) Deep Rolling for Tailoring Residual Stresses of AA2024 Sheet Metals. In: Mocellin K, Bouchard P-O, Bigot R. (eds) Proceedings of the 14th International Conference on the Technology of Plasticity - Current Trends in the Technology of Plasticity: ICTP 2023 - Volume 3, 1st ed. 2024. Springer Nature Switzerland; Imprint Springer, Cham, ISBN 978-3-031-41341-4, pp 352–362
2. Sticchi M, Schnubel D, Kashaev N et al (2014) Review of residual stress modification techniques for extending the fatigue life of

metallic aircraft components. https://doi.org/10.1115/1.4028160. Applied Mechanics Reviews 67
3. Schijve J (ed) (2009) Fatigue of structures and materials. Springer Netherlands, Dordrecht
4. Schajer GS (2013) Practical residual stress measurement methods. Wiley
5. Treuting RG, Read WT Jr (1951) A mechanical determination of biaxial residual stress in sheet materials. J Appl Phys 22:130–134
6. Altenberger I Deep rolling–the past, the present and the future. In: Conf Proc: ICSP, pp 144–155
7. Nagarajan B, Kumar D, Fan Z et al (2018) Effect of deep cold rolling on mechanical properties and microstructure of nickel-based superalloys. Mater Sci Engineering: A 728:196–207. https://doi.org/10.1016/j.msea.2018.05.005
8. Beghini M, Bertini L, Monelli BD et al (2014) Experimental parameter sensitivity analysis of residual stresses induced by deep rolling on 7075-T6 aluminium alloy. Surf Coat Technol 254:175–186. https://doi.org/10.1016/j.surfcoat.2014.06.008
9. Alasvand K (2012) Simulation and research on deep rolling process parameters. ADMT J 5
10. Denkena B, Grove T, Breidenstein B et al (2018) Correlation between process load and deep rolling induced residual stress profiles. Procedia CIRP 78:161–165
11. Kämmler J, Wielki N, Meyer D (2018) Surface integrity after internal load oriented multistage contact deep rolling. Procedia CIRP 71:490–495
12. Kinner-Becker T, Sölter J, Karpuschewski B (2020) A simulation-based analysis of internal material loads and material modifications in multi-step deep rolling. Procedia CIRP 87:515–520
13. Pöltl D, Sala ST, Kashaev N et al Eigenstrain method in simulations of laser peen forming of curved surfaces. Materials Research Proceedings 41:2355–2363. https://doi.org/10.21741/9781644903131-259
14. Dursun T, Soutis C (2014) Recent developments in advanced aircraft aluminium alloys. Mater Des (1980–2015) 56:862–871
15. ASTM (2020) Standard test method for determining residual stresses by the Hole-Drilling Strain-Gage method 77.040.10(E. 837–820. https://doi.org/10.1520/E0837-20
16. Schajer GS, Steinzig M (2005) Full-field calculation of hole drilling residual stresses from electronic speckle pattern interferometry data. Exp Mech 45:526–532. https://doi.org/10.1007/BF02427906
17. Schajer GS, Rickert TJ (2011) Incremental computation technique for residual stress calculations using the integral method. Exp Mech 51:1217–1222
18. Pöltl D, Keller S, Chupakhin S et al (2022) Numerical investigation of influence of spot geometry in laser Peen forming of Thin-Walled Ti-6Al-4V specimens. Key engineering materials. Trans Tech Publications Ltd, pp 2293–2302